# HOKKAIDO UNIVERSITY

| | |
|---|---|
| Title | Wetting failure in the early stage of water drop impact on a smooth solid surface |
| Author(s) | Adachi, Ryunosuke; Kobayashi, Kazumichi; Fujii, Hiroyuki et al. |
| Citation | Physics of fluids, 34(6), 62116<br>https://doi.org/10.1063/5.0096813 |
| Issue Date | 2022-06-22 |
| Doc URL | https://hdl.handle.net/2115/89984 |
| Rights | This article may be downloaded for personal use only. Any other use requires prior permission of the author and AIP Publishing. This article appeared in Ryunosuke Adachi, Kazumichi Kobayashi, Hiroyuki Fujii, Toshiyuki Sanada, and Masao Watanabe, "Wetting failure in the early stage of water drop impact on a smooth solid surface", Physics of Fluids 34, 062116 (2022) and may be found at https://aip.scitation.org/doi/abs/10.1063/5.0096813. |
| Type | journal article |
| File Information | 5.0096813.pdf |

# Wetting failure in the early stage of water drop impact on a smooth solid surface

Ryunosuke Adachi, Kazumichi Kobayashi, Hiroyuki Fujii, et al.

View Online    Export Citation    CrossMark

**ARTICLES YOU MAY BE INTERESTED IN**

**Physics of Fluids**

# Wetting failure in the early stage of water drop impact on a smooth solid surface

Ryunosuke Adachi,[1] (iD) Kazumichi Kobayashi,[1] (iD) Hiroyuki Fujii,[1] (iD) Toshiyuki Sanada,[2] (iD)
and Masao Watanabe[1,a)] (iD)

## AFFILIATIONS

[1]Division of Mechanical and Aerospace Engineering, Hokkaido University, Sapporo 060-8628, Japan
[2]Department of Mechanical Engineering, Shizuoka University, Hamamatsu 432-8561, Japan

[a)]Author to whom correspondence should be addressed: masao.watanabe@eng.hokudai.ac.jp

## ABSTRACT

A water drop impacting a dry solid surface can eject a thin liquid sheet, which is forced to expand on the surface to wet the solid surface. Wetting failure, which produces defects in applications based on the impact of drops, including coating, cooling, cleaning, and printing, may occur with a sufficiently large liquid-sheet velocity. However, the exact onset of wetting failure when a drop impacts the surface has yet to be determined. Therefore, we examine the dependence of rim instability immediately after liquid-sheet ejection on the static contact angle of the solid surface at the instant of water drop impact. This study is the first attempt to solve this problem and is made possible only by using an ultra-high-speed camera. We revealed that wetting failure can occur by investigating the rim instability of the liquid sheet.

*Published under an exclusive license by AIP Publishing.* https://doi.org/10.1063/5.0096813

## I. INTRODUCTION

A fast-moving thin liquid sheet can be ejected across a solid surface when a drop impacts this surface.[1–11] Wetting a solid surface using an ejected liquid sheet is essential in many physical problems and practical applications, including thermal spray coating,[12,13] spray cooling,[14] surface cleaning,[15] fuel injection in internal combustion engines,[16] and ink-jet printing.[17,18] However, wetting may fail, destabilizing the contact line, forcing the dynamic contact angle $\theta_d$ to approach a maximum value of $180°$,[19–21] and causing the entrainment of gas bubbles[22] when the liquid-sheet velocity exceeds the critical velocity. Thus, wetting failure may produce defects in these applications.

Wetting failure, which depends on the static contact angle $\theta_s$ of the solid surface,[23–26] has been suggested to cause splashing.[27] If wetting failure occurs at drop impact, splashing should depend on $\theta_s$. However, certain studies have concluded that the surface wetting properties do not affect the splashing threshold.[28–30] In contrast, others have shown that splashing depends on either $\theta_s$[31] or $\theta_d$.[9] The extent to which splashing depends on $\theta_s$ remains unclear. Thus, to the authors' knowledge, the onset of wetting failure at the instant of drop impact has yet to be elucidated. Importantly, all these studies observed the occurrence of splashing in the late stage of drop impact when $\tau(= tV/R_b)$ was greater than 0.4,[9,29–31] where $V$ is the impact velocity of the drop, $R_b$ is the bottom radius of curvature of the drop, and $t$ is the time after the instant of impact.

In contrast, the occurrences of splashing in the early stage ($\tau < 0.2$) of water drop impact on a smooth glass surface with typical roughness of a few nanometers were observed.[32,33] These results indicate that splashing can be observed in the early stage ($\tau < 0.2$) of water drop impact on a glass surface when the surface is smooth enough. Considering that the liquid-sheet velocity (i.e., the liquid–gas–solid contact-line velocity) can be expressed in proportion to $(\tau^{-1/2})$,[5,32,34,35] the contact-line velocity can become extremely large when $\tau$ is small. This extremely large velocity can exceed the critical velocity to cause wetting failure. Thus, wetting may more likely fail in the early stage ($\tau < 0.2$) than in the late stage ($\tau > 0.4$) of drop impact. The typical shapes of impact drops when $\tau < 0.2$ and $\tau > 0.4$ are shown in Figs. 1(a) and 1(b), respectively.

This study used a Shimadzu HPV-1 ultra-high-speed video camera at a frame rate of up to 1 000 000 fps. We observed the thin liquid sheet ejected at the instant when a water drop impacts a cover glass with a roughness of a few nanometers and the subsequent onset of wetting failure in the early stage ($\tau < 0.2$) of water drop impact. We prepared cover glasses with different wettabilities to examine the $\theta_s$-dependence of the onset of wetting failure. Finally, we discuss the applicability of the proposed theoretical models,[24,36] which explain the dependence of $\theta_d$ on the contact-line velocity of a liquid film on a solid surface with $\theta_s$ in predicting our experimental results.
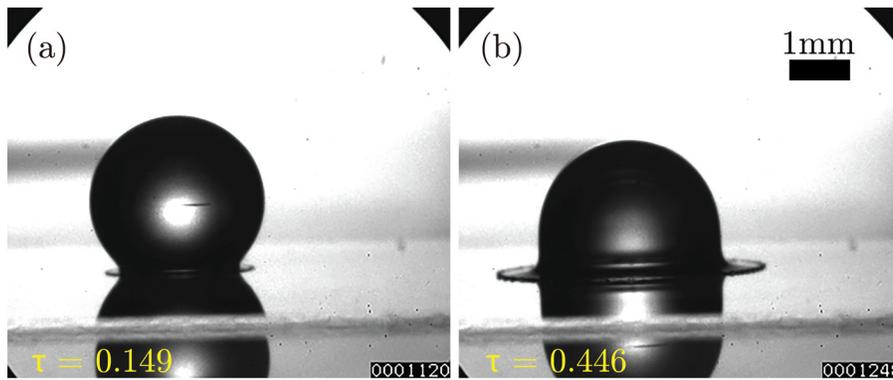
**FIG. 1.** Expansions of a liquid sheet (a) at $\tau = 0.149$ and (b) at $\tau = 0.446$. A water drop with an $R_b$ of 1.46 mm impacting a cover glass with $V$ of 3.39 m/s and $\theta_s$ of 75.8° caused the liquid sheet to expand. Neither wetting failure nor splashing was observed under these conditions.

## II. EXPERIMENT SETUP

A water drop was released from a needle with an inner diameter of 0.41 mm (22G; Terumo needle). Then, the water drop collided with a cover glass (C218181; Matsunami Glass Ind., Ltd.). The impact was observed from underneath the cover glass[32] using a long-distance microscope with a resolution of 23.8 $\mu$m/px. The optical axis of the camera was tilted from the direction of gravity by 20°. We captured the expansion of the liquid sheet at a frame rate of 1 000 000 fps and the occurrence of splashing, which was visually identified when at least one daughter droplet was ejected from the rim of the liquid sheet, at a frame rate of 500 000 fps. Further discussion on exposure time for observing drop impact is provided in Appendix A. The impact velocity $V$ was measured using a NAC HX-3 high-speed video camera at a frame rate of 10 000 fps. Changing the release height from 0.45 to 1.25 m controlled $V$ in the range of 2.9 to 4.6 m/s.

The shape of the drop deforms during the free fall.[34] Assuming the drop had an elliptic shape, the equivalent spherical radius $R_e$ and the bottom radius of curvature $R_b$ were estimated as $R_e = D_v^{1/3} D_h^{2/3}/2$ and $R_b = D_h^2/(2D_v)$, respectively,[34,37] where $D_h$ and $D_v$ were the horizontal and vertical diameters of the drop at impact, respectively. In our experiments, $R_e$ was 1.49 ± 0.0265 mm, and $R_b$ was 1.54 ± 0.137 mm.

The static contact angle $\theta_s$ of the cover glass was measured using a polynomial fitting method.[38] The measured $\theta_s$ values of the surfaces of the non-treated cover glasses were 43.7° ± 3.23° (top face) and 61.5° ± 4.02° (bottom face). The surface roughness $R_a$ (arithmetical mean deviation of the assessed profile) of both top and bottom faces, which were measured using an atomic force microscope (MFP-3D-BIO-J; Asylum Research), were the same: $R_a \sim 2.2$ nm. Some cover glasses were treated with atmospheric nitrogen plasma (P500-SM; Sakigake-Semiconductor Co., Ltd.) to render them more hydrophilic, with $\theta_s$ as small as 6.1°. Others were coated with fluorine resin film (FluoroSurf FS-1600; FluoroTechnology Co., Ltd.) to render them hydrophobic, with $\theta_s$ as large as 109°. Further explanation of plasma treatment of glass surface is provided in Appendix B.

## III. RESULTS
### A. Observation of wetted area and thin liquid sheet

Consecutive images of a water drop impact, observed from underneath the cover glass, are presented in Fig. 2 (Multimedia view). Figures 2(a) (Multimedia view) and 2(b) (Multimedia view) show

those with hydrophobic surface ($\theta_s = 75.8°$), and Fig. 2(c) (Multimedia view) shows those with hydrophilic surface ($\theta_s = 14.4°$). The impact velocities $V$ in these experiments were practically the same.

When the drop impacts the cover glass, a circular wetted area is first observed at $\zeta = 0$. The temporal coordinate $\zeta$ for each drop impact experiment is defined by

$$\zeta = \tau - \tau_0, \qquad (1)$$

where $\tau_0$, which is evaluated in Sec. III C, is a constant for each impact experiment. As this area expands, a thin liquid sheet emerges from the edge of this area (see the inset images in the second column of Fig. 2). Then, the onset of rim instability on the hydrophobic surface is observed [see the inset images in the third column of Figs. 2(a) and 2(b)] in the very early stage of drop impact when $\zeta < 0.09$. This rim instability did not necessarily lead to splashing. In fact, no splashing is observed in Fig. 2(b), although splashing is observed in Fig. 2(a) (see the inset images in the fourth column). In contrast, neither rim instability nor splashing on the hydrophilic surface is observed in Fig. 2(c).

### B. Critical impact velocities

The experimental results highlight that rim instability and splashing depend both on the impact velocity $V$ and the static contact angle $\theta_s$ of the cover glass (Fig. 3). Discriminant analysis based on the Mahalanobis distance[39,40] was used to evaluate the critical impact velocities $V^{crit}$ for rim instability and the threshold impact velocities $V^{spl}$ for splashing. The onset of rim instability occurs when $V$ exceeds $V^{crit}$, and splashing occurs when $V$ exceeds $V^{spl}$.

Both of these velocities, $V^{crit}$ and $V^{spl}$, decrease as $\theta_s$ increases, although no consistent trends in the differences between $V^{crit}$ and $V^{spl}$ are identified. Increasing $V$ increases the liquid-sheet velocity $U$ at the instant of ejection.[5] Thus, the onset of rim instability may occur when this velocity exceeds a critical liquid-sheet velocity $U^{crit}$ that depends on $\theta_s$.

Here, we propose the hypothesis that rim instability at the end of the liquid sheet with a root radius of $A$, which is also a radius of the wetted area, and a tip radius of $R$ (Fig. 4) arises from wetting failure. The contact line of the liquid sheet may be destabilized as the dynamic contact angle $\theta_d$ approaches 180°.[19–21] Predicting the critical impact velocity $V^{crit}$, above which wetting failure occurs, requires an appropriate evaluation of both the velocity $U$ and the thickness $H$ of the
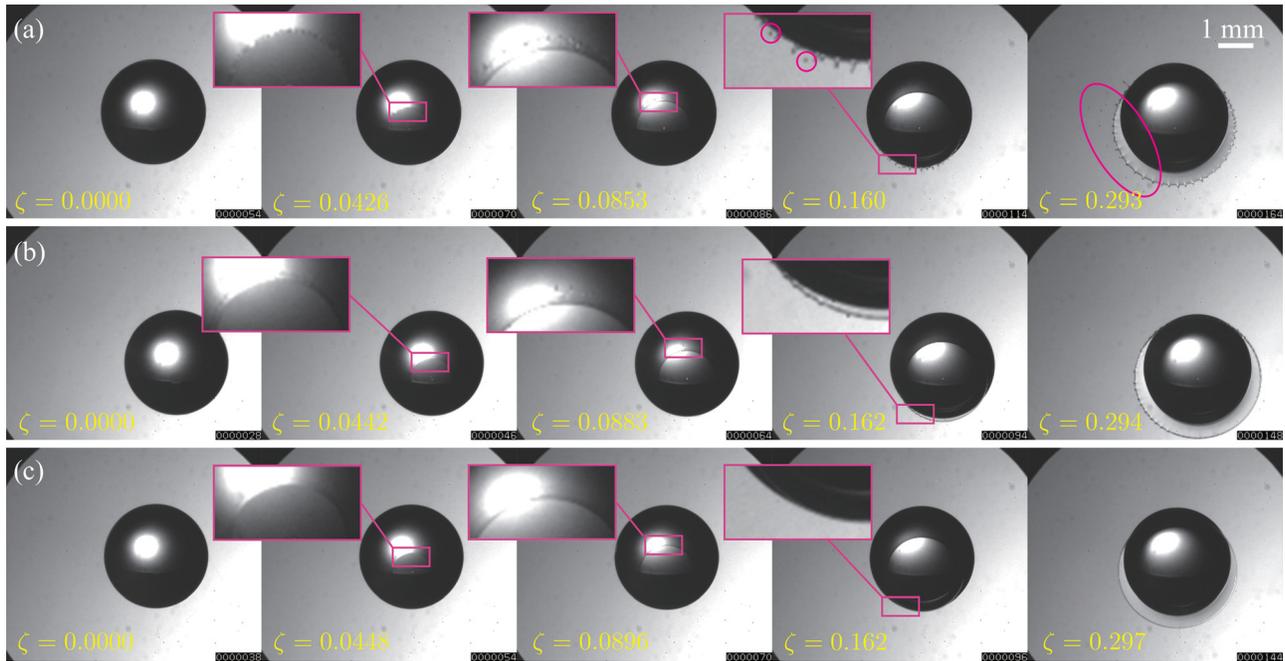
**FIG. 2.** Consecutive images of the wetted area and thin liquid sheet in the early stage of drop impact (a) with the occurrence of splashing: $\theta_s = 75.8°$, $V = 3.73$ m/s, $R_b = 1.40$ mm; (b) with the onset of rim instability: $\theta_s = 75.8°$, $V = 3.70$ m/s, $R_b = 1.50$ mm; and (c) with a smooth liquid sheet: $\theta_s = 14.4°$, $V = 3.75$ m/s, $R_b = 1.34$ mm. The thin liquid sheets after their ejection can be observed in the insets in the second column. Then, fingers can be observed in the insets in the third column of (a) and (b) only. Finally, splashing can only be observed in the inset in the second column of (a). The leftmost image in each row is the first image (when the drop contacts the glass surface) in the sequence of images captured by the ultra-high-speed camera. Thus,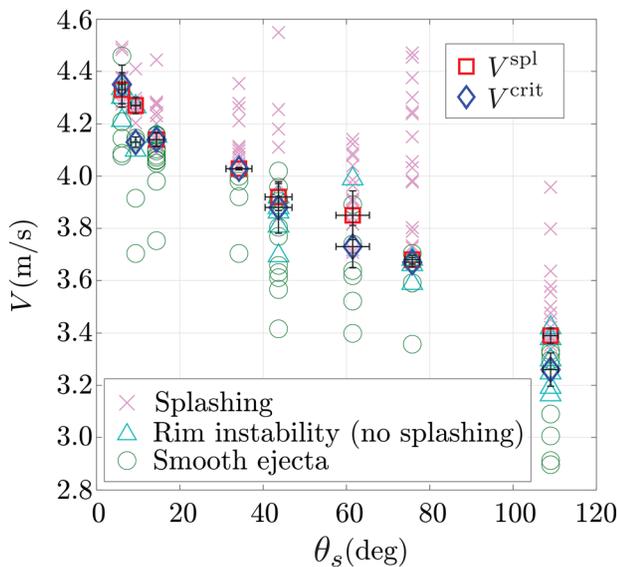 $\zeta = 0$ was assigned to this image. Multimedia views: https://doi.org/10.1063/5.0096813.1; https://doi.org/10.1063/5.0096813.2; https://doi.org/10.1063/5.0096813.3

liquid sheet at the instant of ejection. These radii and thicknesses are made dimensionless using $R_b$, i.e., $a = A/R_b$, $r = R/R_b$, $h = H/R_b$, and the liquid-sheet velocity $U$ is also made dimensionless using $V$, i.e., $u = U/V$.

### C. Expansion of wetted area

The expansions of the wetted area and the liquid sheet were observed using an ultra-high-speed camera with a frame rate of 1 000 000 Hz from underneath the cover glass. Here, $V$ ranged from



**FIG. 3.** Critical impact velocities for rim instability $V^{crit}$ and threshold impact velocities for splashing $V^{spl}$ in terms of the static contact angle $\theta_s$ of the cover glass.
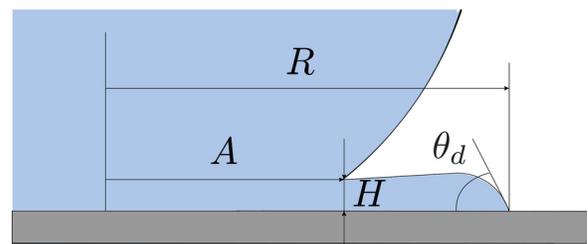


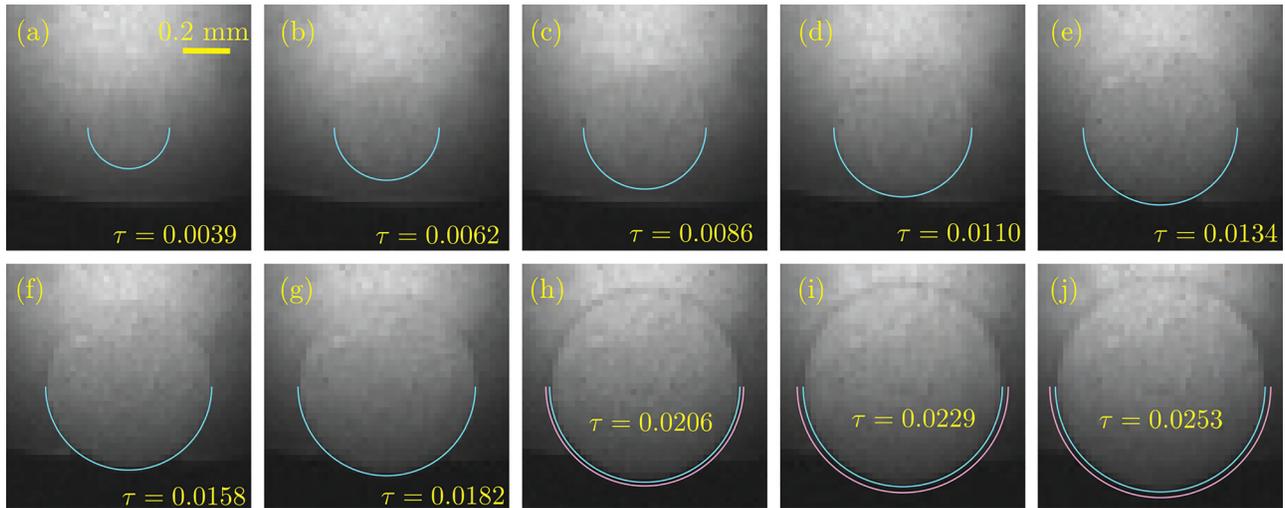**FIG. 4.** Sketch of the geometry of a wetted area and a liquid sheet at the instant of ejection.

**FIG. 5.** Visual identification of the radii of wetted area $a$ (blue line) and the radii of the tip of the liquid sheet $r$ (red line) at (a) $\zeta = 0$, (b) $\zeta = 0.002\,38$, (c) $\zeta = 0.004\,77$, (d) $\zeta = 0.007\,15$, (e) $\zeta = 0.009\,54$, (f) $\zeta = 0.0119$, (g) $\zeta = 0.0143$, (h) $\zeta = 0.0167$, (i) $\zeta = 0.0191$, and (j) $\zeta = 0.0215$ ($V = 3.82$ m/s, $R_b = 1.60$ mm, $\theta_s = 15.9°$).

2.99 to 3.94 m/s, and $\theta_s$ from 8.9° to 49.0°. The optical axis of the camera was tilted from the direction of gravity by 20°. Thus, the original images taken by the camera were distorted, as shown in Fig. 2. Images were stretched only in the vertical axis by $(1/\cos 20°)$ to correct the distortion of images. Thus, corrected images are presented in Fig. 5.

When a drop makes contact with the cover glass, the bottom radius of curvature locally decreases,[41,42] and, thus, a circular wetted area is first observed at $\zeta = 0$ [Fig. 5(a)]. This circular wetted area is fitted with a circle of radius $a$. As the wetted area expands, a liquid sheet expands from the tip of the wetted area. Thus, an annulus darker than the surroundings is observed around the circular wetted area.[32] The width of this annulus increases as the liquid sheet further expands. We define the time when the width of the annulus becomes approximately two pixels as the apparent ejection time $\zeta_e^a$. Then, the outer perimeter of the annulus is fitted by a circle of radius $r$ for $\zeta \geq \zeta_e^a$ [Figs. 5(h)–5(j)].

The expansion of the experimentally obtained radius $a$ of the wetted area can be fitted to a function:[34,35] $a = C_a\sqrt{\zeta + \tau_0}$, where $C_a$ and $\tau_0$ are fitting coefficients. Thus, using Eq. (1), the expansion of $a$ is expressed as follows:

$$a = C_a\sqrt{\tau}. \qquad (2)$$

The experimentally obtained expansion of the radius $a$ of the wetted area shown in Fig. 5 is plotted in Fig. 6 with the apparent ejection time $\tau_e^a$: $\tau_e^a = \zeta_e^a + \tau_0$. The corresponding fitting curve [Eq. (2)], which has been well verified experimentally[34,35] to fit the experimental results, is also drawn. These coefficients $C_a$ and $\tau_0$ are calculated from the results of 33 experiments. These values are tabulated in Table I along with the experimental conditions.

We examine the dependence of the expansions of $a$ on the impact velocity $V$ and the static contact angle $\theta_s$ of the cover glass. First, we examine the dependence of the expansion on $V$, which ranges from 2.99 to 3.94 m/s. The experimental results and corresponding fitted curves are plotted in Fig. 7(a). Three curves in Fig. 7(a) virtually

collapse into one line. This result implies that the expansion of liquid sheet is seemingly independent of $V$ in this range of $V$.

Then, we examine the dependence of the expansion on $\theta_s$, which ranges from 8.9° to 49.0°. The experimental results and corresponding fitted curves are plotted in Fig. 7(b). Three curves in Fig. 7(b) are hardly distinguishable. Thus, this result implies that the expansion of liquid sheet is seemingly independent of $\theta_s$ in this range of $\theta_s$.

These results conclude that the wetted area's expansion appears to be independent of both the impact velocity $V$ and the static contact angle $\theta_s$ of the cover glass. Thus, the fitting coefficient $C_a$ is implied to be a constant independent of both $V$ and $\theta_s$. These experimentally obtained coefficients are averaged to yield $C_a = 1.80 \pm 0.0296$. The
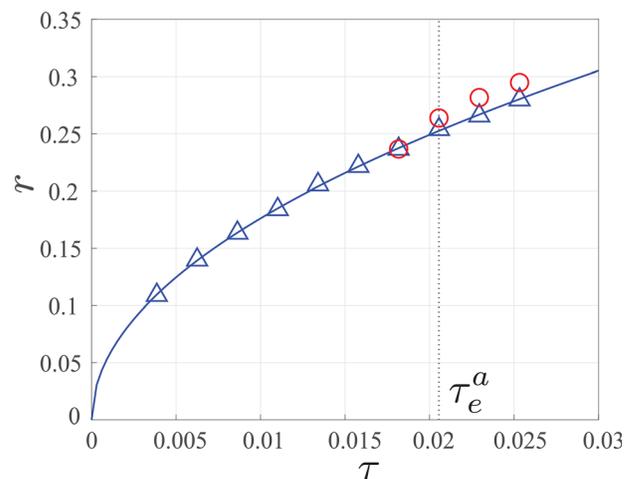


**FIG. 6.** Experimental results of expansions of the radius $a$ of the wetted area (open triangle) and the radius $r$ of the tip of the liquid sheet (open circle) evaluated from Fig. 5 with $\tau_e^a = 0.0206$. The fitted curve to $a$ was obtained as $a(\tau) = 1.76\sqrt{\tau}$ with $\tau_0 = 0.003\,86$. ($V = 3.82$ m/s, $R_b = 1.60$ mm, $\theta_s = 15.9°$.)

**TABLE I.** Fitting coefficients $C_a$ and $\tau_0$ and ejection time $\tau_e$ for the expansion of liquid sheets under the following conditions: $V$ of 2.99 to 3.94 m/s and $\theta_s$ of 8.9° to 49.0°. The experimental data with the conditions in the rows (∗) are plotted in Fig. 7(a), and those in rows (∗∗) are plotted in Fig. 7(b), respectively.

| $\theta_s$ (deg) | $V$ (m/s) | $R_b$ (mm) | $C_a$ | $\tau_0\ (\times 10^{-2})$ | $\tau_e\ (\times 10^{-2})$ | $We$ | |
|---|---|---|---|---|---|---|---|
| 49 | 3.399 | 1.512 | 1.873 | 0.480 | 0.955 | 239 | (∗∗) |
| | 3.406 | 1.566 | 1.820 | 0.557 | 0.901 | 249 | |
| | 3.428 | 1.599 | 1.843 | 0.405 | 0.738 | 258 | |
| | 3.586 | 1.491 | 1.790 | 0.482 | 0.836 | 263 | |
| | 3.621 | 1.450 | 1.822 | 0.603 | 0.877 | 261 | |
| | 3.581 | 1.420 | 1.816 | 0.400 | 0.966 | 250 | |
| | 3.236 | 1.372 | 1.830 | 0.498 | 0.908 | 197 | |
| | 3.209 | 1.333 | 1.821 | 0.395 | 1.143 | 188 | |
| | 3.229 | 1.318 | 1.824 | 0.483 | 1.123 | 188 | |
| 15.9 | 3.013 | 1.718 | 1.791 | 0.423 | 0.809 | 214 | (∗) |
| | 2.993 | 1.580 | 1.800 | 0.405 | 0.915 | 193 | |
| | 3.015 | 1.580 | 1.799 | 0.395 | 0.770 | 197 | |
| | 3.153 | 1.337 | 1.861 | 0.683 | 1.058 | 182 | |
| | 3.202 | 1.397 | 1.794 | 0.749 | 1.035 | 194 | |
| | 3.168 | 1.397 | 1.814 | 0.470 | 0.987 | 192 | |
| | 3.453 | 1.483 | 1.765 | 0.606 | 1.276 | 242 | (∗, ∗∗) |
| | 3.436 | 1.515 | 1.769 | 0.405 | 1.242 | 242 | |
| | 3.433 | 1.515 | 1.777 | 0.594 | 0.967 | 245 | |
| | 3.794 | 1.557 | 1.753 | 0.582 | 1.074 | 307 | |
| | 3.828 | 1.601 | 1.777 | 0.519 | 1.110 | 309 | |
| | 3.818 | 1.601 | 1.761 | 0.386 | 1.213 | 320 | |
| | 3.942 | 1.671 | 1.769 | 0.312 | 0.881 | 356 | (∗) |
| | 3.942 | 1.671 | 1.758 | 0.490 | 0.884 | 349 | |
| | 3.942 | 1.671 | 1.768 | 0.310 | 0.987 | 356 | |
| 8.9 | 3.446 | 1.480 | 1.797 | 0.404 | 0.902 | 241 | (∗∗) |
| | 3.451 | 1.430 | 1.820 | 0.536 | 1.068 | 233 | |
| | 3.396 | 1.353 | 1.827 | 0.683 | 1.041 | 214 | |
| | 3.606 | 1.382 | 1.790 | 0.473 | 0.856 | 246 | |
| | 3.562 | 1.364 | 1.773 | 0.688 | 1.053 | 237 | |
| | 3.576 | 1.420 | 1.784 | 0.601 | 0.921 | 249 | |
| | 3.192 | 1.344 | 1.818 | 0.585 | 1.098 | 188 | |
| | 3.199 | 1.333 | 1.818 | 0.631 | 1.002 | 187 | |
| | 3.231 | 1.364 | 1.809 | 0.594 | 1.041 | 195 | |

variation in these fitting coefficients is similar to that previously observed.[34] Thus, we obtain the following:

$$a(\tau) = 1.80\sqrt{\tau}, \tag{3}$$

in the range of the present experimental conditions. The coefficient in Eq. (3) is approximately equal to $\sqrt{3}$, which was theoretically predicted[43] by solving the Laplace equation and determining $a$ using the Wagner condition. Then, the thickness $h$ of the liquid sheet at the instant of the ejection was derived as[43]

$$h = \left. \frac{a(\tau)}{2\pi(da(\tau)/d\tau)^2} \right|_{\tau=\tau_e}, \tag{4}$$

where $\tau_e$ is the ejection time.

## D. Ejection time

Considering that rim instability is observed in the early stage of drop impact ($\tau < 0.2$), the contact-line velocity $u$ of the liquid sheet at the ejection time $\tau_e$ is the relevant characteristic velocity that dominates this physical process. Hence, an accurate estimation of $\tau_e$ is essential. However, visibly identifying the sheet ejection requires approximately two pixels between the tip and root of the liquid sheet.

To determine $\tau_e$, the condition that $\dot{r}(\tau_e) = \dot{a}(\tau_e)$ is used,[5] where the dot denotes the derivative with respect to $\tau$. This condition leads to that $a(\tau)$ and $r(\tau)$ are tangent to each other at $\tau = \tau_e$. Thus, the liquid-sheet velocity $u$ at the instant of ejection is obtained as

$$u = \left. \frac{da(\tau)}{d\tau} \right|_{\tau=\tau_e} = \frac{C_a}{2\sqrt{\tau_e}}, \tag{5}$$

and $r$ can be assumed to be fitted by the following straight line:

$$r \approx \frac{C_a\sqrt{\tau_e}}{2}\left(1 + \frac{\tau}{\tau_e}\right), \tag{6}$$

in the close neighborhood of $\tau = \tau_e$. Equation (6) represents the line tangent to $a = C_a\sqrt{\tau}$ at $\tau = \tau_e$, where $\tau_e$ is treated as the fitting parameter. Using Matlab curve fitting toolbox, three radii, $a(\tau_e^a - \Delta\tau)$, $r(\tau_e^a)$, and $r(\tau_e^a + \Delta\tau)$, measured from the observation are fitted by Eq. (6), where $\Delta\tau$ is the nondimensional time interval between two consecutive images. The fitted line using data from Fig. 5 are plotted in Fig. 8. The ejection time $\tau_e$ is obtained as the point of contact between the fitted line and $a(\tau) = C_a\sqrt{\tau}$. Thus, evaluated ejection time $\tau_e$ using 33 experimental results are also presented in Table I.

For further examination of the ejection time $\tau_e$, a pair of nondimensional numbers is introduced:

$$We_D = \frac{\rho R_b V^2}{\sigma}, \tag{7}$$

$$Oh_D = \frac{\mu}{\sqrt{\rho R_b \sigma}}, \tag{8}$$

where $\rho = 998$ kg/m³, $\mu = 1.00$ mPa s, and $\sigma = 72.8 \times 10^{-3}$ N/m are the density, viscosity, and surface tension of water, respectively. In our experiments, $180 \lesssim We_D \lesssim 400$ and $Oh_D \simeq 0.003$. These ejection times $\tau_e$ and the visibly identified ejection times $\tau_e^a$ are plotted in Fig. 9, which reveals that $\tau_e$ is apparently independent of $\theta_s$. The ejection time $\tau_e$ was proposed to be proportional to $We_D^{-2/3}$ in the limit that $Oh_D \ll 1$.[44] Thus, the experimental results shown in Fig. 9 suggest that $\tau_e$ can be fitted by

$$\tau_e = 0.370\,We_D^{-2/3}. \tag{9}$$

Consequently, the velocity $u$ and the thickness $h$ of the liquid sheet at the instant of ejection can be calculated using Eqs. (5) and (4), respectively.

$$u = 1.48\,We_D^{1/3}, \tag{10}$$

$$h = 0.0796\,We_D^{-1}. \tag{11}$$

The dimensional velocity $U$ and thickness $H$ are, thus, obtained as $U = uV$ and $H = hR_b$, respectively.
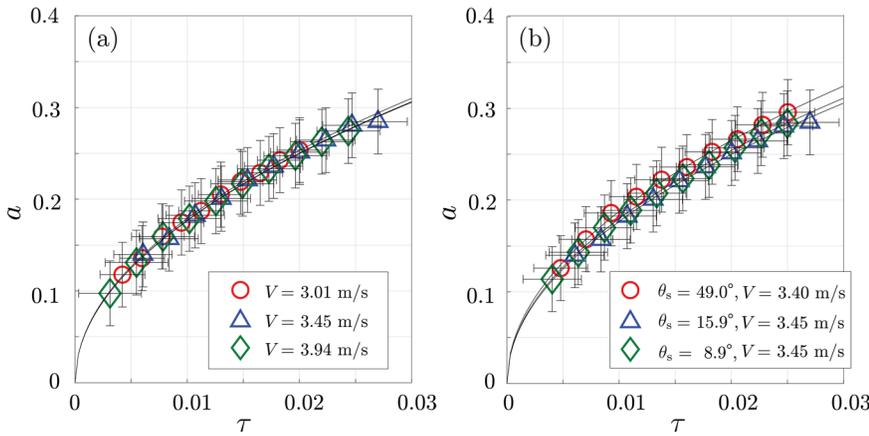
**FIG. 7.** Expansions of the radii $a(\tau)$ of the wetted area. The experimentally obtained radii were fitted using (2): $a(\tau) = C_a\sqrt{\tau}$. Expansions of $a$ (a) on cover glasses with $\theta_s$ of 15.9° and with various $V$, and (b) on cover glasses with various $\theta_s$ and with $V$ of approximately 3.4 m/s.

## IV. DISCUSSION

### A. Wetting failure in the early stage of water drop impact

We investigate the $\theta_s$-dependence of the liquid-sheet instability using theoretical models proposed by Cox.[24,36] These models can predict the dependence of the dynamic contact angle $\theta_d$ on the liquid-sheet velocity $U$ at the instant of ejection of a liquid sheet with a thickness of $H$. Three nondimensional numbers are introduced in these models:

$$Ca = \frac{\mu U}{\sigma} = 1.48\, Oh_D We_D^{5/6}, \tag{12}$$

$$Re = \frac{\rho U H}{\mu} = 0.127\, Oh_D^{-4/5} Ca^{-1/5}, \tag{13}$$

$$\varepsilon = \frac{S}{H} = 7.85\left(\frac{S}{R_b}\right) Oh_D^{-6/5} Ca^{6/5}, \tag{14}$$

where $S$ is the slip length and Eqs. (10) and (11) are used. The characteristic impact velocity can be defined as 3.8 m/s, which is the midpoint of the range of $V^{\text{crit}}$ (approximately between 3.2 and 4.4 m/s) in Fig. 3, and the characteristic bottom radius of curvature is 1.54 mm. Thus, the characteristic nondimensional numbers $We_D^c$, $Ca^c$, and $Re^c$ are 305, 0.520, and 15.1, respectively. The viscosity ratio $\lambda = \mu_g/\mu$, where $\mu_g$ is the viscosity of air, is also used in the following analysis. The standard viscosity ratio $\lambda_0$ is defined as 0.0181.

The contact line of the liquid sheet may be destabilized as $\theta_d$ approaches 180°.[19–21] Thus, the critical capillary number above which wetting failure occurs may be predicted using the Cox theory with $\theta_d$ of 180°. Note that this predicted capillary number may give an upper limit for the critical capillary number considering that the contact line of the liquid sheet may be destabilized when $\theta_d < 180°$.[45,46]

Cox[36] investigated the dynamics involved in the movement of the contact line for the viscous-dominated situation. First, he investigated the asymptotic form of the velocity field in both the liquid and
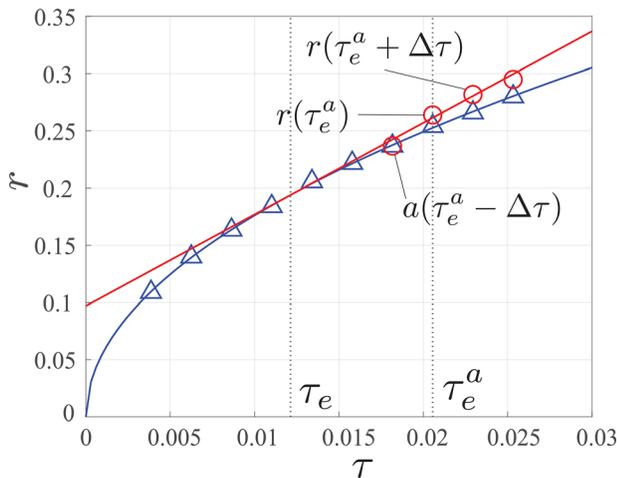


**FIG. 8.** Fitted line to the experimental results measured from Fig. 5 ($V = 3.82$ m/s, $R_b = 1.60$ mm, $\theta_s = 15.9°$). The fitted curve for the radius of the wetted area: $a(\tau) = 1.76\sqrt{\tau}$, and the fitted straight line for the tip of the liquid sheet in the close neighborhood of $a(\tau_e)$ where $\tau_e = 0.0121$: $r(\tau) = 8.00(\tau + 0.0121)$.
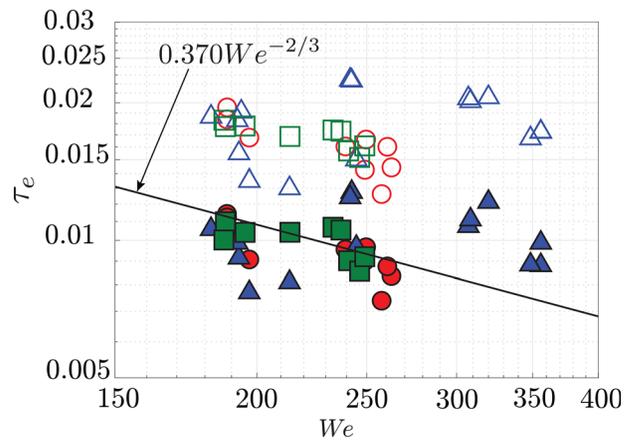


**FIG. 9.** Experimentally obtained ejection time $\tau_e$ with various $We_D$ ($= \rho V^2 R_b/\sigma$) plotted in log-log scale. The results obtained after making an impact with the glasses for $\theta_s = 49.0°$, 15.9°, and 8.9° are denoted by circles, triangles, and squares, respectively. The open symbols denote the apparent ejection time $\tau_e^a$. The closed symbols denote the ejection time $\tau_e$ that was evaluated using Eq. (6). The solid line denotes the fitted line [Eq. (9)].

gas phases as $r \to 0$ in the plane polar co-ordinates $(r, \phi)$, where the plane $\phi = \theta_d$ is at rest and the plane $\phi = 0$ is scraped along parallel to itself. This is well-known as Taylor's scraping problem.[47,48] He

solved the Stokes equation for the stream function $\psi(r, \phi)$, $\nabla^4 \psi = 0$, which admits separated solutions of the form $\psi = r^{-1} \varphi(\phi)$. He found the normal stress on the interface $\phi = \theta_d$ to be $f(\theta_d, \lambda)/r$, where

$$f(\theta, \lambda) = \frac{2 \sin \theta \left[ \lambda^2 (\theta^2 - \sin^2 \theta) + 2\lambda \{ \theta(\pi - \theta) + \sin^2 \theta \} + \{ (\pi - \theta)^2 - \sin^2 \theta \} \right]}{\lambda(\theta^2 - \sin^2 \theta) \{ (\pi - \theta) + \sin \theta \cos \theta \} + \{ (\pi - \theta)^2 \sin^2 \theta \}(\theta - \sin \theta \cos \theta)}. \tag{15}$$

Then, using matched asymptotic expansion, Cox found that a third region, the intermediate region of expansion, must exist between the inner and outer expansion regions to connect them. Thus, he obtained the dependence of $\theta_d$ on the contact line velocity over the solid surface

$$Ca \ln (\varepsilon^{-1}) = g_v(\theta_d) - g_v(\theta_s), \tag{16}$$

where

$$g_v(\theta) = \int_0^\theta \frac{\mathrm{d}x}{f(x, \lambda)}. \tag{17}$$

With $\theta_d = 180°$ and $\lambda = \lambda_0$, and both $\theta_s$ and $\varepsilon$ specified, the critical capillary number can be evaluated through Eq. (16). This critical capillary number is referred to as $Ca^{\mathrm{I}}$.

Later, Cox[24] examined the more general situation,

$$1 \le Re \le \varepsilon^{-1}. \tag{18}$$

In this situation, viscous effects become more dominant in the intermediate region asymptotically closer to the inner region. Conversely, the flow becomes more inviscid in the intermediate region that is asymptotically closer to the outer region. Furthermore, he subdivided the intermediate region into viscous sub-region, transition sub-region, and inviscid sub-region. The more detailed explanation of the regions of asymptotic expansion by Cox is provided in Appendix C.

In a transition sub-region, the liquid interface shape must be of the form $\theta = \theta^* + Ca\theta_1^* + \cdots$, where $\theta^*$ is a constant contact angle in the intermediate region, but $\theta_1^*$ is a function of radial distance from the contact line in the transition sub-region. In the inviscid sub-region, he obtained

$$Ca \ln (Re) = g_{iv}(\theta_d) - g_{iv}(\theta^*), \tag{19}$$

where

$$g_{iv}(\theta) = 1.53162(\theta - \sin \theta). \tag{20}$$

Likewise, in the viscous sub-region, he obtained

$$Ca \ln (\varepsilon^{-1} Re^{-1}) = g_v(\theta^*) - g_v(\theta_s). \tag{21}$$

With $\theta_d = 180°$ and $\lambda = \lambda_0$, and both $\theta_s$ and $\varepsilon$ specified, the critical capillary number along with $\theta^*$ can also be evaluated as solutions of a pair of simultaneous nonlinear equations [Eqs. (19) and (21)]. This critical capillary number is referred to as $Ca^{\mathrm{II}}$.

The slip length $S$, which can be less than 2 nm,[49] should be determined. However, the proposed values of $S$ may be distributed across a wide range.[50,51] Thus, $S$ in this model is instead treated as a parameter to fit the experimental data.[26,52]

We examine the experimental results using these critical capillary numbers $Ca^{\mathrm{I}}$ with $S = 28$ nm and $Ca^{\mathrm{II}}$ with $S = 1.8$ nm. These predicted critical capillary numbers $Ca^{\mathrm{I}}$ and $Ca^{\mathrm{II}}$ for wetting failure agree well with each other (Fig. 10). Note that the values of $S$ and $Re^c$ satisfy the condition [Eq. (18)], which guarantees the applicability of the Cox theory to this study. The critical capillary number for rim instability $Ca^{\mathrm{crit}} = 1.48\, Oh_D (We_D^{\mathrm{crit}})^{5/6}$ $(We_D^{\mathrm{crit}} = \mu V^{\mathrm{crit}}/\sigma)$ and the threshold capillary number for splashing $Ca^{\mathrm{spl}} = 1.48\, Oh_D (We_D^{\mathrm{spl}})^{5/6}$ $(We_D^{\mathrm{spl}} = \mu V^{\mathrm{spl}}/\sigma)$ are also presented.

The important finding in Fig. 10 is that $Ca^{\mathrm{crit}}$ reaches up to approximately 0.65, which is much larger than the one that Cox assumed. He assumed $Ca \ll 1$ in his analysis. The accuracy and applicability of the Cox theory for $Ca > 0.1$ remains debated.[25,26,53–55] However, numerical analysis[26] would indicate that the overall trend of the sensitivity of the critical capillary number to $\theta_s$ for liquid-sheet movement in the air can be well described by the Cox theory even up to $Ca \approx 1$. Thus, the Cox theory may be applicable to predicting the critical capillary numbers.
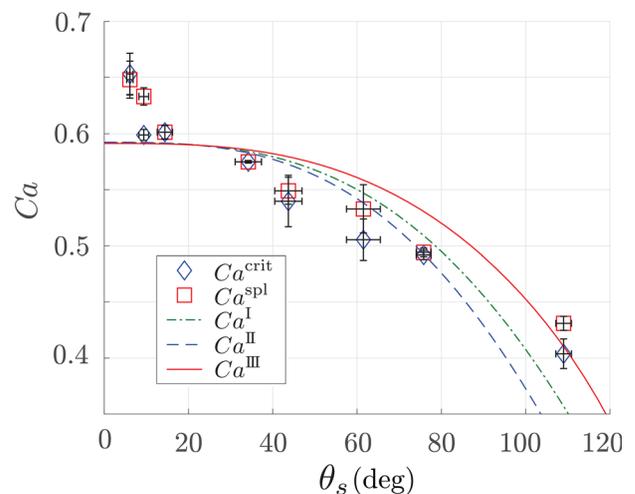


**FIG. 10.** Onset of wetting failure: predicted and experimental results. The critical capillary number for rim instability $Ca^{\mathrm{crit}} = \mu u V^{\mathrm{crit}}/\sigma$ (diamond) and the threshold capillary number for splashing $Ca^{\mathrm{spl}} = \mu u V^{\mathrm{spl}}/\sigma$ (square) were calculated from experiment results. The critical capillary number $Ca^{\mathrm{I}}$ (dash-dot line) was calculated using Eq. (16), and the critical capillary number $Ca^{\mathrm{II}}$ (dashed line) was calculated using Eqs. (19) and (21) with $\lambda_0 = \mu_g/\mu = 0.0181$. The critical capillary number $Ca^{\mathrm{III}}$ (solid line) using $\lambda = \mu_e/\mu$ in Eq. (17), where $\mu_e$ is evaluated from Eq. (23), well describes the overall trend of $\theta_s$-dependency of $Ca^{\mathrm{crit}}$.

The role of the viscosity of the gas is investigated to further understand $\theta_s$-dependency of $Ca^{II}$. The effective viscosity $\mu_e$ is well known to depend on the Knudsen number $Kn$ $(= \ell_g/L^c)$[56] when $Kn$ becomes large, and to decrease to zero as $Kn \to \infty$,[57,58] where $\ell_g$ is the mean-free-path of the air ($\ell_g \simeq 70$ nm) and $L^c$ is the characteristic length scale of the flow. The flow is viscous-dominated in the viscous sub-region [Eq. (21)], whereas the flow is irrotational in the inviscid sub-region [Eq. (19)]. Thus, the characteristic lengthscale of transition sub-region $H/Re$[24] seems to be suitable for $L^c$, and the relevant Knudsen number $Kn$ is written as

$$Kn = \left(\frac{\ell_g}{R_b}\right) Oh_D^{-2} Ca, \qquad (22)$$

and hence, $2.03 \lesssim Kn \lesssim 3.30$.

The effects of $Kn$ on gas viscosity were investigated using the Direct Simulation Monte Carlo method for $0.1 \leq Kn \leq 10$.[58] The dependence of gas viscosity on $Kn$ can be well fitted by a Bosanquet-type of approximation:[58,59]

$$\mu_e = \mu_g \frac{1}{1 + \xi Kn}, \qquad (23)$$

where $\xi$ was proposed to be equal to 2. Thus, $\mu_e$ $(0.132\mu_g \lesssim \mu_e \lesssim 0.198\mu_g)$ may be an appropriate evaluation for this analysis. With, thus, evaluated $\mu_e$ instead of $\mu_g$ in Eq. (17), another critical capillary number can be evaluated. This critical capillary number is referred to as $Ca^{III}$. This critical capillary number $Ca^{III}$ with $S = 0.9$ nm is plotted in Fig. 10. This critical capillary number can well describe the overall trend of $\theta_s$-dependency of $Ca^{crit}$.

In Sec. III B, we proposed the hypothesis that the rim instability of the liquid sheet observed in the early stage ($\tau < 0.2$) of water drop impact arises from wetting failure when a water drop impacts a smooth, dry glass surface with $R_a \sim 2.2$ nm. Our finding that $Ca^{III}$ can well predict $Ca^{crit}$ provides some evidence that can support this hypothesis. The critical capillary number above which this rim instability occurs can be predicted using the Cox theory. These results conclude that wetting failure can occur in the early stage ($\tau < 0.2$) of water drop impact on a smooth glass surface with $R_a \sim 2.2$ nm.

## B. Splashing in the early stage of water drop impact

We observed splashing in the early stage ($\tau < 0.2$) of water drop impact on a smooth glass surface with $R_a \sim 2.2$ nm in Fig. 2. To better understand this splashing that arises from wetting failure, we examine whether this splashing can be predicted by the splashing threshold using the splashing ratio $\beta$ proposed by Riboux and Gordillo.[5] The gas layer under the liquid sheet causes a vertical lift force per unit length $F_L$ that exerts on the edge of the liquid sheet. This lift force generates a vertical velocity $U_v$ to the liquid sheet: $U_v \propto \sqrt{F_L/(\rho H)}$. The capillary retraction causes the radial growth of the liquid-sheet rim. The characteristic velocity $U_r$ can be given by $U_r \propto \sqrt{2\sigma/(\rho H)}$. Riboux and Gordillo[5] assumed that the liquid sheet separates from the surface when $U_v$ is larger than $U_r$. Thus, they proposed that splashing occurs when the splashing ratio $\beta$,

$$\beta = \sqrt{\frac{F_L}{2\sigma}}, \qquad (24)$$

exceeds $\beta^{\text{thld}}$ that is the threshold value of $\beta$. Riboux and Gordillo[5] evaluated $F_L$ using the lubrication approximation, and then, experimentally obtained that $\beta^{\text{thld}}$ ranged from 0.12 to 0.14.[5,44,60]

Later, de Goede et al.[29] simplified Eq. (24) and evaluated $\beta$ for low $Oh_D$ at atmospheric conditions

$$\beta = \left(\frac{2.22}{\tan \alpha}\right) \frac{\mu_g^{1/2}(\rho R_b V^5)^{1/6}}{\sigma^{2/3}}, \qquad (25)$$

where $\alpha$ is the wedge angle between the lifted sheet and the surface. This $\alpha$ was assumed to be a constant. This constant is independent of the condition in the vicinity of the liquid–solid contact.[44] Also, $\alpha$ was reported to be independent of the surface wettability.[29] Thus, $\beta^{\text{thld}}$ was suggested to be independent of the surface wettability. The commonly used value of $\alpha$ is 60°.[29,43] They experimentally obtained that $\beta^{\text{thld}}$ ranged between 0.11 and 0.14.

We examine whether $\beta^{\text{thld}}$ can be estimated from the results obtained in Sec. IV A. The lift force per unit length $F_L$ in Eq. (24) can be approximated as proportional to $\mu_g U$.[43,61] Thus, $\beta \propto \sqrt{\lambda_0 Ca}$. In fact, using Eq. (12), Eq. (25) can be rewritten as follows:

$$\beta = 1.05\sqrt{\lambda_0 Ca}. \qquad (26)$$

Thus, evaluating $\beta^{\text{thld}}$ for splashing observed in the early stage ($\tau < 0.2$) of water drop impact on a smooth glass surface at atmospheric conditions using Eq. (25) would seem to be equivalent to evaluating the threshold capillary number for splashing $Ca^{\text{spl}}$. Both Riboux and Gordillo[5] and Cox[24,36] studied the viscous gas flow near the tip of the liquid sheet and the deformation of the gas–liquid interface using the solution of either the scraping problem[24,36] or the lubrication problem.[5]

Considering that $Ca^{\text{spl}}$ can be well predicted by the critical capillary numbers ($Ca^{I}$, $Ca^{II}$, and $Ca^{III}$) as shown in Fig. 10, we calculated $\beta^{\text{thld}}$ for splashing observed in the early stage ($\tau < 0.2$) of water drop
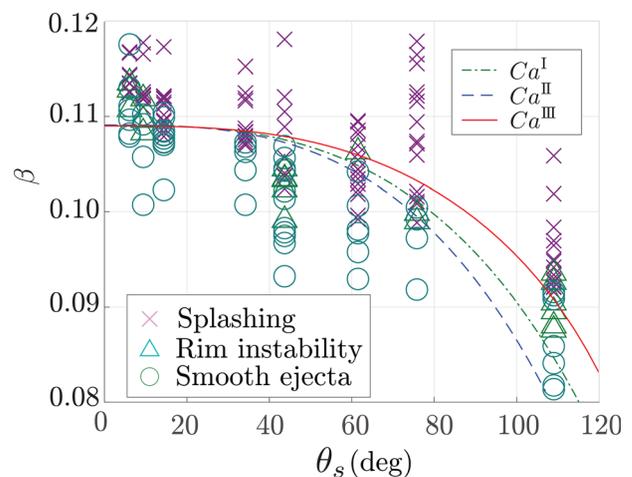
**FIG. 11.** Splashing ratio $\beta$ in terms of the static contact angle $\theta_s$ of the cover glass. The splashing ratio $\beta$ for splashing observed in the early stage ($\tau < 0.2$) of water drop impact on a smooth glass surface corresponding to the experimental data that are shown in Fig. 3 are calculated by using Eq. (25). The threshold $\beta^{\text{thld}}$ s corresponding to the critical capillary numbers ($Ca^{I}$, $Ca^{II}$, and $Ca^{III}$) that are shown in Fig. 10 are calculated by using Eq. (26).
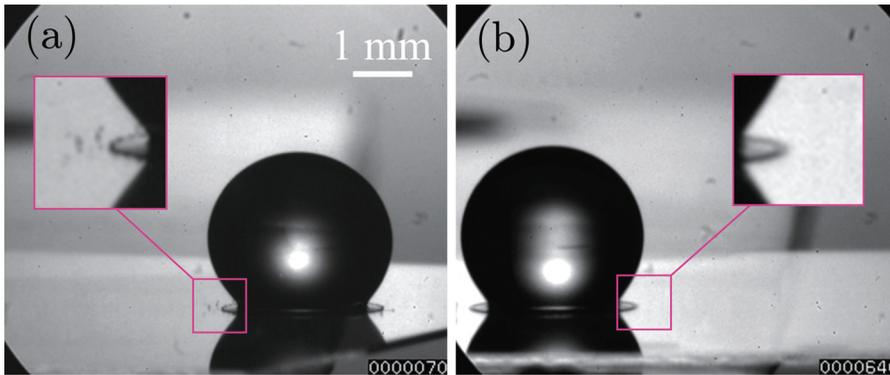
**FIG. 12.** Images of water drop impact on a cover glass of $\theta_s = 37.8°$ with different exposure times. (a) $V = 4.38$ m/s, $R_b = 1.67$ mm, exposure time of 1 $\mu$s, and frame rate = 500 kfps. $\tau = 0.14$. (b) $V = 4.37$ m/s, $R_b = 1.59$ mm, exposure time was 8 $\mu$s, and frame rate = 63 kfps. $\tau = 0.14$. Multimedia views: https://doi.org/10.1063/5.0096813.4; https://doi.org/10.1063/5.0096813.5

impact on a smooth glass surface by substituting the critical capillary numbers plotted in Fig. 10 into Eq. (26). We also calculated the splashing ratio $\beta$ by substituting experimental data in Fig. 3 into Eq. (25). They are plotted in Fig. 11.

The static contact angle $\theta_s$ obviously affects $\beta^{\text{thld}}$ for splashing observed in the early stage ($\tau < 0.2$) of water drop impact on a smooth glass surface at atmospheric conditions. Decreasing $\theta_s$ increases $\beta^{\text{thld}}$ (Fig. 11). The range of $\beta^{\text{thld}}$ observed in the early stage ($\tau < 0.2$) of water drop impact on a smooth glass surface is that $0.9 \lesssim \beta^{\text{thld}} \lesssim 1.1$. This $\beta^{\text{thld}}$ would seem significantly less than those previously reported.[5,29,44,60] Moreover, daughter droplets ejected from the rim of the liquid sheet appear to fly along the glass surface as observed in Fig. 12 (Multimedia view) in Appendix B, which indicates that the wedge angle $\alpha$ is much less than 60°.

These results may suggest that the splashing criterion [Eq. (24)] that can predict the occurrence of previously investigated splashing cannot predict splashing observed in the early stage ($\tau < 0.2$) of water drop impact on a smooth glass surface at atmospheric conditions.

### C. Dependence of splashing on surface wetting properties

We examine the difference in the extent to which splashing depends on the surface wetting properties between splashing observed in the early stage ($\tau < 0.2$) and splashing observed in the late stage ($\tau > 0.4$).[9,28–31] Interestingly, de Goede et al.[29] showed that the surface wetting properties do not influence $\beta^{\text{thld}}$ by examining the dependence of the occurrence of splashing on the surface wetting properties when an ethanol–water mixture drop impacted a dry surface. They found that the best fit value of $\beta^{\text{thld}}$ the ethanol–water mixtures equals $0.120 \pm 0.008$ using three different surfaces, each having roughness $R_a < 500$ nm, and thus, $\gamma \sim 1$, where $\gamma$ is the ratio of surface roughness $R_a$ to the liquid-sheet thickness $H$ ($\gamma = R_a/H$).

In contrast, we used the cover glass surfaces, having roughness $R_a \sim 2.2$ nm, and thus, $\gamma \ll 1$. Garcia-Geijo et al.[62] showed that the larger $\gamma$ should destabilize the liquid sheet. They further indicated that fingers with a typical diameter $\sim R_a$ protrude with no smooth liquid sheet formed when $\gamma \gtrsim 1$. The large difference in $\gamma$ would seem to suggest that surface roughness should dominate wettability in causing splashing observed by de Goede et al.,[29] who observed no splashing within the velocity range investigated ($0.1 < V < 4.7$ m/s) for pure water drop impact.

Although the influence of surface roughness on splashing has been studied,[62–65] the interplay between the surface wettability and surface roughness in the dynamics of splashing remains largely unclear.[62,66] This interplay is a vital issue for further studies of drop impact splashing.

The dependence of $\beta^{\text{thld}}$ on the maximum advancing contact angle $\theta_{\max}$ was examined by Quetzeri-Santiago et al.[9] for ethanol, water, and an aqueous glycerol solution with $\theta_s$ ranging from 0° to 140°. They obtained that $\beta^{\text{thld}} = -0.0011\theta_{\max} + 0.23$ (thus, $\beta^{\text{thld}} \approx 0.11$–$0.13$ for surfaces with $\theta_{\max}$ ranging from 83° to 103°. This range of $\beta^{\text{thld}}$ also significantly greater than our result. They used various surfaces: glass, ultraclean mica, glaco-coated surfaces, perfluorodecyl acrylates (PFAC), and polytetrafluoroethylene (PTFE). Although no explicit descriptions of surface roughness were provided in their study, a smooth surface made of synthetic resin, in general, would seem to be much rougher than the surface of the cover glass with a surface roughness of $R_a \sim 2.2$ nm. For example, a plastic cover glass made of polyvinyl chloride (PL100; Thermo Fisher Scientific) has $R_a \sim 31.2$ nm surface roughness. This result indicates that some of the surfaces that Quetzeri-Santiago et al.[9] used probably had much larger $R_a$ than our cover glass surface. Thus, again, the difference in $\gamma$ suggests that surface roughness should be responsible for the difference in the extent to which splashing depends on the surface wetting properties.

Surprisingly, Quetzeri-Santiago et al.[9] indicated that this splashing occurred in the late stage ($\tau > 0.4$) of drop impact when the liquid sheet might be thick enough [Fig. 1(b)] for $\theta_d$ to be measured from images. In contrast, we observed splashing only in the early stage ($\tau < 0.2$) of drop impact when the liquid sheet was too thin [Fig. 1(a)] for $\theta_d$ to be measured. In addition, the liquid-sheet velocity can be approximately expressed in proportion to $\tau^{-1/2}$. Thus, the liquid-sheet velocity in the late stage ($\tau > 0.4$), which should be much smaller than that in the early stage ($\tau < 0.4$), would seem to be too small to cause wetting failure.

These results allow us to conclude that surface roughness dominates surface wettability in the previously investigated splashing in the late stage ($\tau > 0.4$) of drop impact. Thus, the dependence of splashing in the early stage ($\tau < 0.2$) of water drop impact on the surface wettability has been first identified. Furthermore, this splashing depends on the surface wettability through the static contact angle $\theta_s$ of the surface.

### V. CONCLUSIONS

The rim instability at the end of the thin liquid sheet ejected and subsequent splashing in the early stage ($\tau < 0.2$) of water drop impact

on a smooth cover glass surface with a roughness of a few nanometers depends on the surface wettability through the static contact angle $\theta_s$ of the cover glass. Reducing $\theta_s$ through plasma treatment increases the critical impact velocity for rim instability and, thus, suppresses splashing. The observation using the ultra-high-speed camera with 1 000 000 fps indicated that the expansion of liquid sheet is independent of the impact velocity $V$ and the static contact angle $\theta_s$ of the cover glass. Thus, the ejection time $\tau_e$ was implied as $\tau_e = 0.370 We_D^{-2/3}$ regardless of $\theta_s$ in the range of the present experimental conditions.

Using these results with the Cox theory[24,36] for wetting failure, we examined the $\theta_s$-dependence of the critical capillary number for rim instability $Ca^{\mathrm{crit}}$. Our study showed that the Cox theory can reasonably predict the experimental results. Thus, we have identified that wetting failure can occur in the early stage ($\tau < 0.2$) of water drop impact. Examining the roughness of the surfaces used in the previous studies[9,29] suggested that the ratio of surface roughness to the liquid-sheet thickness possibly explains the difference in the extent to which the threshold capillary number for splashing depends on the surface wetting properties. Thus, further studies will explore the interplay between surface wetting properties and surface roughness. The present findings may have important implications for practical applications, including coating, cooling, cleaning, and printing, where wetting solid surfaces using the liquid sheet ejected when a liquid drop impacts the solid surface is essential.

## AUTHOR DECLARATIONS
### Conflict of Interest

The authors have no conflicts to disclose.

### Author Contributions

**Ryunosuke Adachi:** Conceptualization (equal); Data curation (lead); Formal analysis (equal); Investigation (equal); Methodology (equal); Software (equal); Validation (equal); Visualization (lead); Writing – original draft (equal); Writing – review and editing (equal). **Kazumichi Kobayashi:** Conceptualization (equal); Investigation (equal); Methodology (equal); Writing – original draft (supporting); Writing – review and editing (supporting). **Hiroyuki Fujii:** Conceptualization (equal); Investigation (equal); Methodology (equal); Writing – original draft (supporting); Writing – review and editing (supporting). **Toshiyuki Sanada:** Conceptualization (equal); Investigation (equal); Methodology (equal); Writing – original draft (supporting); Writing – review and editing (supporting). **Masao Watanabe:** Conceptualization (equal); Data curation (supporting); Formal analysis (equal); Funding acquisition (lead); Investigation (equal); Methodology (equal); Project administration (lead); Resources (lead); Software (equal); Supervision (lead); Validation (equal); Visualization (supporting); Writing – original draft (equal); Writing – review and editing (equal).

## APPENDIX A: EXPOSURE TIME FOR OBSERVING DROP IMPACT

The extremely short exposure time of less than 1 $\mu$s of the ultra-high-speed camera enabled us to observe wetting failure clearly when $\tau < 0.2$ and to evaluate the remarkably short ejection time $\tau_e$ accurately. Few efforts to observe wetting failure and subsequent splashing in the early stage of drop impact have been reported. These phenomena can only be observed with an ultra-high-speed video camera. Thoroddsen et al.[32] observed splashing at the instant of drop impact with a solid surface when $\tau < 0.05$, using an ultra-high-speed video camera with a frame rate of 500 kfps. They found that daughter droplets with radii of several tens of $\mu$m are ejected at velocities of several tens of m/s. This result may suggest that the exposure time should be a few microseconds to prevent the images of the fast-moving daughter droplets from being blurred. Thus, we examined whether a longer exposure time may lead to failure in observing splashing.

First, a drop impact with $V$ of 4.38 m/s on a cover class with $\theta_s$ of 37.8° was observed using an ultra-high-speed video camera with an exposure time of 1 $\mu$s. This exposure time enabled the observation of splashing at $\tau = 0.14$, as shown in Fig. 12(a) (Multimedia view). The inset of Fig. 12(a) shows ejected daughter droplets, although the images of the droplets are blurred. Then, a drop impact with $V$ of 4.37 m/s on the same cover glass was observed using the same ultra-high-speed video camera with an exposure time of 8 $\mu$s. Although the experimental conditions were virtually the same as those of the previous experiment, this long exposure time indeed led to the failure to observe splashing, as shown in Fig. 12(b) (Multimedia view). Figure 3 in the main text indicates that splashing on the cover glass with $\theta_s$ of 37.8° can be observed when $V \geq 4.0$ m/s. However, no ejected daughter droplets could be identified in the inset of Fig. 12(b).

A comparison of these two observations reveals that an exposure time of approximately 1 $\mu$s would be required to observe splashing in the early stage of drop impact. This restriction on the exposure time may have been the reason for the scarcity of reports. This extremely short exposure time required to observe wetting failure may have hindered the investigation of the dependence of splashing on the surface wetting properties when $\tau < 0.2$. Previous studies appeared to observe the occurrence of splashing when $\tau > 0.4$.[9,29–31]

## APPENDIX B: PLASMA TREATMENT OF GLASS SURFACE

The hydrophilicity of some of the cover glasses was increased by exposing them to nitrogen plasma using a pen-type nitrogen
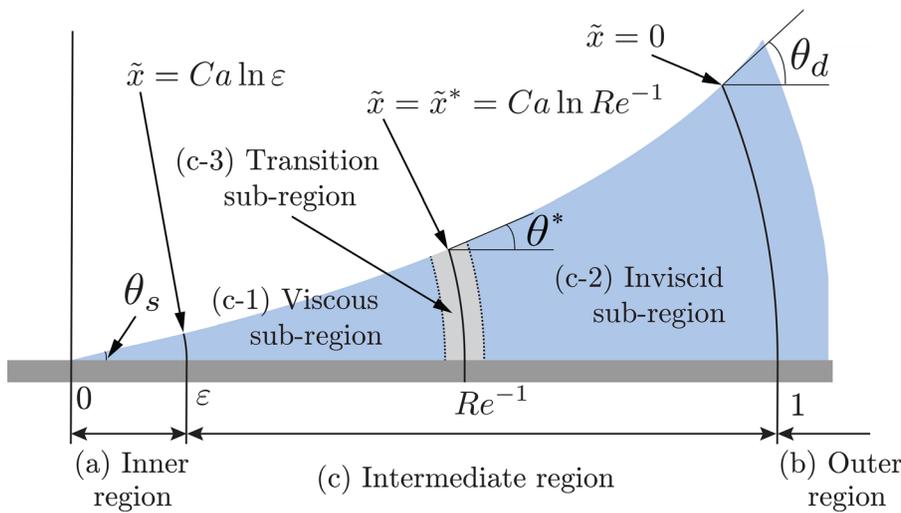
**FIG. 13.** The regions of matched asymptotic expansion used by Cox[24] near the contact line of the liquid film.

plasma device at atmospheric pressure (P500-SM; Sakigake-Semiconductor Co., Ltd.). A cover glass was placed underneath the plasma pen, which directed the plasma onto the glass surface, with a standoff distance of 20 mm from the tip of the plasma pen. Increasing the plasma irradiation time $t_{pi}$ decreased the contact angle: $\theta_s = 75.8°$ ($t_{pi} = 0$ s), $34.2°$ (2 s), $14.4°$ (4 s), $9.4°$ (6 s), $6.1°$ (8 s). Thus, the surface wettability was modified. The decrease in $\theta_s$ lasted more than 15 min.

Modification of the surface wettability by using plasma treatment was further investigated. We used x-ray photoelectron spectroscopy (XPS; JPC-9010MC, JEOL Ltd.) to identify the elements on the surface as their chemical states. This spectroscopy can measure the intensity of the photoemission corresponding to the chemical bonding.

The results of the XPS measurements indicated that increasing the plasma irradiation time $t_{pi}$ decreased the intensity of the photoemission corresponding to the C (carbon) 1s state at 285 eV. Thus, the glass surface became more hydrophilic with larger $t_{pi}$, which may be attributed to the reduction in carbon contamination on the surface. The wettability state is well known to correlate strongly with the surface carbon content.[67–69] Practically, carbon contamination lowers the surface energy, which also increases the hydrophobicity of the surface.[69] In addition, the XPS measurements also indicated that increasing $t_{pi}$ increased the intensity of the photoemission corresponding to the O (oxygen) 1s state at 531 eV.

Exposure to plasma may also change the topological structure of glass surfaces. This structure can determine the wettability of the surface.[70,71] The topological structure of the glass surfaces was observed using atomic force microscopy (AFM; MFP-3D-BIO-J, Asylum Research). The arithmetic mean roughness $R_a$ of the non-treated surface was 2.1 nm whereas $R_a$ of the surface with $t_{pi} = 5$ s was 2.6 nm, and that with $t_{pi} = 30$ s was 3.1 nm. These results indicated that exposure to plasma for less than 10 s did not significantly affect the topological structure of the surface. Hence, changes in the topological structure of the glass surface as a result of plasma treatment may hardly affect the expansion of the liquid sheet.

## APPENDIX C: THE REGIONS OF ASYMPTOTIC EXPANSION BY COX

Cox[24] introduced three regions of expansions and made the distance $X$ dimensionless by characteristic lengthscale $H$: $x = X/H$ (Fig. 13): (a) inner region ($x \sim \varepsilon$), where the flow satisfies the Stokes equation with slip boundary condition applicable on the solid surface; (b) outer region ($x \sim 1$), where a boundary layer region valid near solid boundaries and an inviscid flow region valid elsewhere; and (c) intermediate region ($\varepsilon \lesssim x \lesssim 1$). The contact angles $\theta_s$, $\theta_d$, and $\theta^*$ are defined in the inner, outer, and intermediate regions, respectively.

Then, Cox introduced another length coordinates $\tilde{x} = Ca \ln x$, and thus he subdivided the intermediate region into three subregions: (c-1) viscous sub-region ($Ca \ln \varepsilon \lesssim \tilde{x} \lesssim \tilde{x}^*$) with $\tilde{x}^* = Ca \ln Re^{-1}$, where the flow is viscous-dominated with the velocity and pressure satisfying the Stokes equations and this flow must be matched onto the viscous dominated flow in the inner region as $\tilde{x} \to Ca \ln \varepsilon$ from above; (c-2) inviscid sub-region ($Ca \ln Re^{-1} \lesssim \tilde{x} \lesssim 0$), where the flow is a high Reynolds number flow consisting of an irrotational flow with a boundary layer at the solid surface, and this flow must be matched onto the irrotational flow and boundary layer in the outer region as $\tilde{x} \to 0$ from below; and (c-3) transition sub-region ($\tilde{x} \sim \tilde{x}^*$), where viscous and inertia effects are of the same order, and the solution matches onto the viscous subregion with $\tilde{x} \to \tilde{x}^*$ from below as $r^* \to 0$, and the solution matches onto the inviscid sub-region with $\tilde{x} \to \tilde{x}^*$ from above as $r^* \to \infty$, where $r^* = \exp\{Ca^{-1}(\tilde{x} - \tilde{x}^*)\}$.

## REFERENCES

[1] A. L. Yarin, "Drop impact dynamics: Splashing, spreading, receding, bouncing," Annu. Rev. Fluid Mech. **38**, 159–192 (2006).

[2] S. T. Thoroddsen, T. Etoh, and K. Takehara, "High-speed imaging of drops and bubbles," Annu. Rev. Fluid Mech. **40**, 257–285 (2008).

[3] A. Mongruel, V. Daru, F. Feuillebois, and S. Tabakova, "Early post-impact time dynamics of viscous drops onto a solid dry surface," Phys. Fluids **21**, 032101 (2009).

[4] S. Mandre and M. P. Brenner, "The mechanism of a splash on a dry solid surface," J. Fluid Mech. **690**, 148–172 (2012).

[5]G. Riboux and J. M. Gordillo, "Experiments of drops impacting a smooth solid surface: A model of the critical impact speed for drop splashing," Phys. Rev. Lett. **113**, 024507 (2014).

[6]C. J. Howland, A. Antkowiak, J. R. Castrejón-Pita, S. D. Howison, J. M. Oliver, R. W. Style, and A. A. Castrejón-Pita, "It's harder to splash on soft solids," Phys. Rev. letters **117**, 184502 (2016).

[7]C. Josserand and S. T. Thoroddsen, "Drop impact on a solid surface," Annu. Rev. Fluid Mech. **48**, 365–391 (2016).

[8]S. Lejeune, T. Gilet, and L. Bourouiba, "Edge effect: Liquid sheet and droplets formed by drop impact close to an edge," Phys. Rev. Fluids **3**, 083601 (2018).

[9]M. A. Quetzeri-Santiago, K. Yokoi, A. A. Castrejón-Pita, and J. R. Castrejón-Pita, "Role of the dynamic contact angle on splashing," Phys. Rev. Lett. **122**, 228001 (2019).

[10]M. Broom and G. R. Willmott, "Water drop impacts on regular micropillar arrays: The impact region," Phys. Fluids **34**, 017115 (2022).

[11]N. D. Patil, J. Shaikh, A. Sharma, and R. Bhardwaj, "Droplet impact dynamics over a range of capillary numbers and surface wettability: Assessment of moving contact line models and energy budget analysis," Phys. Fluids **34**, 052119 (2022).

[12]S. D. Aziz and S. Chandra, "Impact, recoil and splashing of molten metal droplets," Int. J. Heat Mass Transfer **43**, 2841–2857 (2000).

[13]Y. Wang, Y. Bai, K. Wu, J. Zhou, M. G. Shen, W. Fan, H. Y. Chen, Y. X. Kang, and B. Q. Li, "Flattening and solidification behavior of in-flight droplets in plasma spraying and micro/macro-bonding mechanisms," J. Alloys Compd. **784**, 834–846 (2019).

[14]G. Liang and I. Mudawar, "Review of spray cooling— Part 1: Single-phase and nucleate boiling regimes, and critical heat flux," Int. J. Heat Mass Transfer **115**, 1174–1205 (2017).

[15]T. Sanada and M. Watanabe, "Photoresist and thin metal film removal by steam and water mixed spray," J. Photopolym. Sci. Technol. **28**, 289–292 (2015).

[16]D. Markt, Jr., M. Raessi, A. Pathak, S.-Y. Lee, and R. Torelli, "Impact of high-speed diesel drop trains - pursuing cleaner diesel engines," Phys. Rev. Fluids **6**, 110508 (2021).

[17]D. B. Van Dam and C. L. Clerc, "Experimental study of the impact of an ink-jet printed droplet on a solid substrate," Phys. Fluids **16**, 3403–3414 (2004).

[18]E. Antonopoulou, O. G. Harlen, M. Rump, T. Segers, and M. A. Walkley, "Effect of surfactants on jet break-up in drop- on-demand inkjet printing," Phys. Fluids **33**, 072112 (2021).

[19]R. Ablett, "An investigation of the angle of contact between paraffin wax and water," London, Edinburgh, Dublin Philos. Mag. J. Sci. **46**, 244–256 (1923).

[20]C. Duez, C. Ybert, C. Clanet, and L. Bocquet, "Making a splash with water repellency," Nat. Phys. **3**, 180–183 (2007).

[21]E. A. Vandre, M. S. Carvalho, and S. Kumar, "Delaying the onset of dynamic wetting failure through meniscus confinement," J. Fluid Mech. **707**, 496–520 (2012).

[22]R. Burley and R. Jolly, "Entrainment of air into liquids by a high speed continuous solid surface," Chem. Eng. Sci. **39**, 1357–1372 (1984).

[23]O. V. Voinov, "Hydrodynamics of wetting," Fluid Dyn. **11**, 714–721 (1976).

[24]R. Cox, "Inertial and viscous effects on dynamic contact angles," J. Fluid Mech. **357**, 249–278 (1998).

[25]T. D. Blake, "The physics of moving wetting lines," J. Colloid Interface Sci. **299**, 1–13 (2006).

[26]E. A. Vandre, M. S. Carvalho, and S. Kumar, "On the mechanism of wetting failure during fluid displacement along a moving substrate," Phys. Fluids **25**, 102103 (2013).

[27]M. Rein and J.-P. Delplanque, "The role of air entrainment on the outcome of drop impact on a solid surface," Acta Mech. **201**, 105–118 (2008).

[28]I. V. Roisman, L. Opfer, C. Tropea, M. Raessi, J. Mostaghimi, and S. Chandra, "Drop impact onto a dry surface: Role of the dynamic contact angle," Colloids Surf., A **322**, 183–191 (2008).

[29]T. C. de Goede, N. Laan, K. G. de Bruin, and D. Bonn, "Effect of wetting on drop splashing of Newtonian fluids and blood," Langmuir **34**, 5163–5168 (2018).

[30]A. Latka, A. M. Boelens, S. R. Nagel, and J. J. de Pablo, "Drop splashing is independent of substrate wetting," Phys. Fluids **30**, 022105 (2018).

[31]D. G. K. Aboud and A. M. Kietzig, "Splashing threshold of oblique droplet impacts on surfaces of various wettability," Langmuir **31**, 10100–10111 (2015).

[32]S. T. Thoroddsen, K. Takehara, and T. Etoh, "Micro-splashing by drop impacts," J. Fluid Mech. **706**, 560–570 (2012).

[33]T. Ashida, M. Watanabe, K. Kobayashi, H. Fujii, and T. Sanada, "Hidden prompt splashing by corona splashing at drop impact on a smooth dry surface," Phys. Rev. Fluids **5**, 011601 (2020).

[34]E. Q. Li, M. J. Thoraval, J. O. Marston, and S. T. Thoroddsen, "Early azimuthal instability during drop impact," J. Fluid Mech. **848**, 821–835 (2018).

[35]J. M. Gordillo, G. Riboux, and E. S. Quintero, "A theory on the spreading of impacting droplets," J. Fluid Mech. **866**, 298–315 (2019).

[36]R. Cox, "The dynamics of the spreading of liquids on a solid surface. Part 1. Viscous flow," J. Fluid Mech. **168**, 169–194 (1986).

[37]M.-J. Thoraval, K. Takehara, T. G. Etoh, and S. T. Thoroddsen, "Drop impact entrapment of bubble rings," J. Fluid Mech. **724**, 234–258 (2013).

[38]E. Albert, B. Tegze, Z. Hajnal, D. Zámbó, D. P. Szekrényes, A. Deák, Z. Hórvölgyi, and N. Nagy, "Robust contact angle determination for needle-in-drop type measurements," ACS Omega **4**, 18465–18471 (2019).

[39]R. de Maesschalck, D. Jouan-Rimbaud, and D. Massart, "The Mahalanobis distance," Chemom. Intell. Lab. Syst. **50**, 1–18 (2000).

[40]R. G. Brereton and G. R. Lloyd, "Re-evaluating the role of the Mahalanobis distance measure," J. Chemom. **30**, 134–143 (2016).

[41]R. C. A. Van Der Veen, T. Tran, D. Lohse, and C. Sun, "Direct measurements of air layer profiles under impacting droplets using high-speed color interferometry," Phys. Rev. E **85**, 026315 (2012).

[42]H. Y. Lo, Y. Liu, and L. Xu, "Mechanism of contact between a droplet and an atomically smooth substrate," Phys. Rev. X **7**, 021036 (2017).

[43]Please see supplementary material in Ref. 5.

[44]G. Riboux and J. M. Gordillo, "Boundary-layer effects in droplet splashing," Phys. Rev. E **96**, 013105 (2017).

[45]Please see supplementary material in Ref. 9.

[46]A. Deblais, R. Harich, A. Colin, and H. Kellay, "Taming contact line instability for pattern formation," Nat. Commun. **7**, 12458 (2016).

[47]G. I. Taylor, "On scraping viscous fluid from a plane surface," in *The Scientific Papers of Sir Geoffrey Ingram Taylor. Volume 4. Mechanics of Fluids: Miscellaneous Papers*, edited by G. Batchelor (Cambridge University Press, Cambridge, 1971), pp. 410–413.

[48]H. K. Moffatt, "Viscous and resistive eddies near a sharp corner," J. Fluid Mech. **18**, 1–18 (1964).

[49]A. Maali, T. Cohen-Bouhacina, and H. Kellay, "Measurement of the slip length of water flow on graphite surface," Appl. Phys. Lett. **92**, 053101 (2008).

[50]E. Lauga, M. P. Brenner, and H. A. Stone, "Microfluidics: The no-slip boundary condition," in *Springer Handbook of Experimental Fluid Mechanics*, edited by C. Tropea, A. L. Yarin, and J. F. Foss (Springer, Berlin, Heidelberg, 2005), pp. 1219–1240.

[51]B. Ramos-Alvarado, S. Kumar, and G. P. Peterson, "Hydrodynamic slip length as a surface property," Phys. Rev. E **93**, 023101 (2016).

[52]C. Y. Liu, M. S. Carvalho, and S. Kumar, "Dynamic wetting failure in curtain coating: Comparison of model predictions and experimental observations," Chem. Eng. Sci. **195**, 74–82 (2019).

[53]M. Y. Zhou and P. Sheng, "Dynamics of immiscible-fluid displacement in a capillary tube," Phys. Rev. Lett. **64**, 882–885 (1990).

[54]Q. Chen, E. Ramé, and S. Garoff, "The breakdown of asymptotic hydrodynamic models of liquid spreading at increasing capillary number," Phys. Fluids **7**, 2631–2639 (1995).

[55]T. S. Chan, C. Kamal, J. H. Snoeijer, J. E. Sprittles, and J. Eggers, "Cox-Voinov theory with slip," J. Fluid Mech. **900**, A8 (2020).

[56]S. Chapman and T. G. Cowling, *The Mathematical Theory of Non-uniform Gases*, 3rd ed. (Cambridge University Press, Cambridge, 1991).

[57]W. Crookes, "VII. On the viscosity of gases at high exhaustions," Phil. Trans. R. Soc. **172**, 387–446 (1881).

[58]V. K. Michalis, A. N. Kalarakis, E. D. Skouras, and V. N. Burganos, "Rarefaction effects on gas viscosity in the Knudsen transition regime," Microfluid. Nanofluid. **9**, 847–853 (2010).

[59]W. G. Pollard and R. D. Present, "On gaseous self-diffusion in long capillary tubes," Phys. Rev. **73**, 762–774 (1948).

[60]J. Hao and S. I. Green, "Splash threshold of a droplet impacting a moving substrate," Phys. Fluids **29**, 012103 (2017).

[61]J. M. Gordillo and G. Riboux, "A note on the aerodynamic splashing of droplets," J. Fluid Mech. **871**, R3 (2019).

[62]P. Garcia-Geijo, E. S. Quintero, G. Riboux, and J. M. Gordillo, "Spreading and splashing of drops impacting rough substrates," J. Fluid Mech. **917**, A50 (2021).

[63]L. Xu, L. Barcos, and S. R. Nagel, "Splashing of liquids: Interplay of surface roughness with surrounding gas," Phys. Rev. E **76**, 066311 (2007).

[64]J. Hao, "Effect of surface roughness on droplet splashing," Phys. Fluids **29**, 122105 (2017).

[65]T. de Goede, K. de Bruin, N. Shahidzadeh, and D. Bonn, "Droplet splashing on rough surfaces," Phys. Rev. Fluids **6**, 043604 (2021).

[66]J. Shen and X. Wang, "Substrate counts: Quantitative effects of surface roughness on fingering pattern and rim shape of an impacting drop," Phys. Fluids **32**, 093313 (2020).

[67]Y. C. Araujo, P. G. Toledo, V. Leon, and H. Y. Gonzalez, "Wettability of silane-treated glass slides as determined from x-ray photoelectron spectroscopy," J. Colloid Interface Sci. **176**, 485–490 (1995).

[68]L. So, N. Ng, M. Bilek, P. J. Pigram, and N. Brack, "X-ray photoelectron spectroscopic study of the surface chemistry of soda-lime glass in vacuum," Surf. Interface Anal. **38**, 648–651 (2006).

[69]Y. Chen, Z. Zhao, and Y. Liu, "Wettability characteristic of PTFE and glass surface irradiated by keV ions," Appl. Surf. Sci. **254**, 5497–5500 (2008).

[70]R. N. Wenzel, "Resistance of solid surfaces to wetting by water," Ind. Eng. Chem. **28**, 988–994 (1936).

[71]A. B. D. Cassie and S. Baxter, "Wettability of porous surfaces," Trans. Faraday Soc. **40**, 546–551 (1944).